Soil Dynamics and Earthquake Engineering 83 (2016) 18–32

Contents lists available at ScienceDirect

Soil Dynamics and Earthquake Engineering

journal homepage: www.elsevier.com/locate/soildyn

Closed form solution of Eigen frequency of monopile supported offshore wind turbines in deeper waters incorporating stiffness of substructure and SSI

Laszlo Arany [a], S. Bhattacharya [b,*], John H.G. Macdonald [a], S. John Hogan [a]

[a] University of Bristol, United Kingdom
[b] Chair in Geomechanics, University of Surrey, United Kingdom

ARTICLE INFO

Article history:
Received 2 September 2015
Received in revised form
13 December 2015
Accepted 17 December 2015
Available online 19 January 2016

Keywords:
Eigen value
Monopile
Deeper water
Beam theory
Soil–structure interaction

ABSTRACT

Offshore wind turbines (OWTs) are dynamically loaded structures and therefore the estimation of the natural frequency is an important design calculation to avoid resonance and resonance related effects (such as fatigue). Monopiles are currently the most used foundation type and are also being considered in deeper waters (> 30 m) where a stiff transition piece will join the monopile and the tapered tall tower. While rather computationally expensive, high fidelity finite element analysis can be carried to find the Eigen solutions of the whole system considering soil–structure interaction; a quick hand calculation method is often convenient during the design optimisation stage or conceptual design stage. This paper proposes a simplified methodology to obtain the first natural frequency of the whole system using only limited data on the WTG (Wind Turbine Generator), tower dimensions, monopile dimensions and the ground. The most uncertain component is the ground and is characterised by two parameters: type of ground profile (i.e. soil stiffness variation with depth) and the soil stiffness at one monopile depth below mudline. In this framework, the fixed base natural frequency of the wind turbine is first calculated and is then multiplied by two non-dimensional factors to account for the foundation flexibility (i.e. the effect of soil–structure interaction). The theoretical background behind the model is the Euler–Bernoulli and Timoshenko beam theories where the foundation is idealised by three coupled springs (lateral, rocking and cross-coupling). 10 wind turbines founded in different ground conditions from 10 different wind farms in Europe (e.g. Walney, Gunfleet sand, Burbo Bank, Belwind, Barrow, Kentish flat, Blyth, Lely, Thanet Sand, Irene Vorrink) have been analysed and the results compared with the measured natural frequencies. The results show good accuracy (errors below 3.5%). A step by step sample calculation is also shown for practical use of the proposed methodology.

1. Introduction

Offshore wind turbines (OWTs) are currently installed in high numbers in Northern Europe and the industry is rapidly developing worldwide. For example, countries such as China, South Korea, Taiwan and Japan are currently developing wind farms and the US has just installed its first pilot offshore wind farm. The Levelised Cost of Energy (LCoE) and SCoE (Society's Cost of Energy) from offshore wind are expected to decrease significantly in the near future and challenging projects in further offshore and deeper water depths (30–50 m), with heavier/larger wind turbines (upwards of 6 MW, with turbines of 10 MW in the testing phase) are underway. OWTs are expected to have a fatigue life of 25–30 years, while foundations are typically designed to last even longer (50 years).

It has been well established that offshore wind turbines are dynamically sensitive structures [10–12,3,35], and dynamics of OWTs must be studied to avoid unplanned resonance which may lead to increased fatigue damage through dynamic amplification of responses. Estimation of the natural frequency of the whole system is an important design calculation [25] so as to avoid the excitation frequencies arising from wind turbulence loading, wave loading, the rotational frequency of the turbine (1P) and the blade passing frequency (2P/3P). The installed number of these relatively new structures is likely to grow significantly in deeper waters and will pose additional dynamic challenges, and is therefore the focus of the paper. Specifically, the paper tackles the issue of the extra length of the tower in water (which is generally stiffer than the tower exposed in air) due to deeper water sites which makes the

* Corresponding author. Tel.: +44 1483 689534.
E-mail addresses: S.Bhattacharya@surrey.ac.uk, Subhamoy.Bhattacharya@gmail.com (S. Bhattacharya).

http://dx.doi.org/10.1016/j.soildyn.2015.12.011

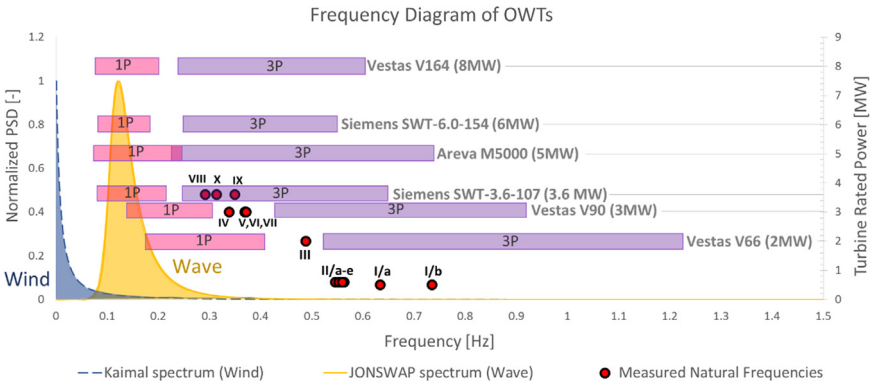

Fig. 1. Typical wind and wave spectra, rotational speed (1P) and blade passing (3P) frequency bands for six commercial turbines and measured natural frequencies of the OWTs given in Table 1.

tower relatively more flexible as compared to shallow water installations thereby lowering the natural frequency of the whole system.

Fig. 1 shows typical wind and wave power spectral densities for offshore sites which essentially describe the frequency content of dynamic excitations from wind turbulence and waves. The graphs also show the turbine's rotational frequency range (1P) and the turbine's blade passing frequency range (3P) for a range of commercial wind turbines of different capacities (2–8 MW). A simplified way of translating the wind turbulence spectrum and the wave spectrum into mudline bending moment spectra through linear transfer functions has been presented in [8]. The peak frequencies of loading have been shown to coincide with the peak frequencies of wind turbulence and waves. However, loads at the 1P and 3P frequencies can also be observed through effects such as aerodynamic and mass imbalance of the rotor and rotational sampling of turbulence by the blades, for 1P and 3P loads, respectively [18,8]. Further details on the estimations of the loads can be found in [13].

For the widely used soft–stiff design, the target Eigen frequency (first natural frequency) is a frequency in the gap between 1P and 3P. Fig. 1 also shows measured natural frequencies of a wide array of OWTs from several different wind farms across Europe (see Table 1 for the nomenclature on the wind turbine structure for which the measured natural frequency is shown and Table 5 for the specification of the turbines given in Fig. 1). The figure clearly shows the trend that the target natural frequencies of heavier turbines are indeed closer to the excitation frequencies of the wave and wind making these structures even more sensitive to dynamics.

1.1. Dynamic issues in support structure design

Fig. 2 shows a schematic diagram of a wind turbine system along with the mechanical model relevant to the study of the overall system dynamics which is important for many design calculations such as Eigen frequencies and fatigue. The definitions of *support structure*, *tower*, *substructure, foundation (monopile considered here), transition piece, mudline* and *mean sea level* are defined in Fig. 2(a) and are consistently used throughout the paper. For clarity, the support structure is the whole structure that supports the heavy turbine i.e. the components below the rotor nacelle assembly (RNA) which includes the tower, substructure and foundation. The foundation is defined as the part of the support structure that is embedded in the ground below the mudline. The tower is typically a tubular tapered column. As the natural frequencies of these systems are very close to the forcing frequencies, the dynamics pose multiple design challenges and the scale of the challenges will vary depending on turbine types and site characteristics. These issues are briefly mentioned in the next section.

There are two main categories of modern wind turbines based on the operational range:

(1) *Variable rotational speed machines* have an operational speed range (1P range);
(2) *Constant rotational speed wind turbines* that operate at a single rotational speed (fixed 1P).

Variable speed machines have 1P and 2P/3P frequency bands which must be avoided, as opposed to a single frequency (applicable to constant rotational speed machines). They are more restrictive from the point of view of foundation design as the forcing frequency is a band rather than a unique value. The turbines currently used in practice (under operation) are variable speed machines. Fig. 1 shows the 1P and 3P bands for typical offshore wind turbines ranging from 2 MW (not in production anymore) turbines to commercially not yet available 8 MW turbines. It may be observed from Fig. 1 that for most wind turbines, 1P and 3P excitation cover wide frequency bands. To avoid these ranges, the designer of the support structure has three options from the point of view of the stiffness of the tower and the foundation [32]:

(1) Soft–soft structures: whereby the natural frequency lies below the 1P frequency range. This design is typical for floating offshore platforms, but are practically impossible to achieve for fixed (grounded) structures. Also, soft–soft fixed structures would likely be subject to high dynamic amplification of wave load response.
(2) Soft–stiff structures: whereby the natural frequency lies above the 1P frequency range. This is the typical design choice for practical bottom fixed structures, such as monopile founded OWTs. All wind turbines in Fig. 1 are designed soft–stiff.
(3) Stiff–stiff structures: whereby the natural frequency lies above the 3P range. Such designs are typically considered to have a massive support structure and therefore uneconomic. However, the Hornsea twisted jacket foundation supporting a met mast has recently successfully achieved a natural frequency above the 3P band [36].

It is quite clear from Fig. 1 that designing a soft–stiff system which avoids both the 1P and 3P frequency bands is challenging because of the tight tolerance of the target natural frequency. Indeed, some OWTs with a wide rotational speed range, such as the Areva M5000 5 MW in Fig. 1 with 4.5–14.8 rpm do not even have a gap between 1P and 3P and they are overlapping. Modern wind turbines often feature a sophisticated pitch control system

Table 1
Analysed offshore wind farms with the used wind turbines and soil conditions at the sites.

No.	Wind farm name and location	Turbine type and rated power	Soil conditions at the site	Data and measured frequency sources
I.	Lely Offsore Wind Farm (Netherlands)	NedWind 40/500 2-bladed 500 kW study purpose wind turbine	Soft clay in the uppermost layer to dense and very dense sand layers below	Zaaijer [54,55] Lindoe Offshore Renewables Center [34]
II.	Irene Vorrink Offshore Wind Farm (Netherlands)	Nordtank NTK600/43 600 kW study purpose wind turbine	Soft layers of silt and clay in the upper seabed to dense and very dense sand below	Zaaijer [54,55] Lindoe Offshore Renewables Center [34]
III.	Blyth Offshore Wind Farm (UK)	Vestas V66 2 MW industrial offshore wind turbine	Rocky seabed (weathered bedrock)	Camp et al. [19] Lindoe Offshore Renewables Center [34]
IV.	Kentish Flats Offshore Wind Farm (UK)	Vestas V90 3 MW industrial offshore wind turbine	Layers of dense sand and firm clay	Damgaard et al. [22] Lindoe Offshore Renewables Center [34]
V.	Barrow Offshore Wind Farm (UK)	Vestas V90 3 MW industrial offshore wind turbine	Layers of dense sand and stiff clay	Damgaard et al. [22] Lindoe Offshore Renewables Center [34]
VI.	Thanet Offshore Wind Farm (UK)	Vestas V90 3 MW industrial offshore wind turbine	Fine sand and stiff clay	Damgaard et al. [22] Lindoe Offshore Renewables Center [34]
VII.	Belwind 1 Offshore Wind Farm (Belgium)	Vestas V90 3 MW industrial offshore wind turbine	Dense sand and stiff clay	Damgaard et al. [22] Lindoe Offshore Renewables Center [34]
VIII.	Burbo Bank Offshore Wind Farm (UK)	Vestas V90 3 MW industrial offshore wind turbine	Saturated dense sand	Versteijlen et al. [52] Lindoe Offshore Renewables Center [34]
IX.	Walney 1 Offshore Wind Farm (UK	Siemens SWT-3.6-107 3.6 MW industrial offshore wind turbine	Medium and dense sand layers	Lindoe Offshore Renewables Center [34] 4C Offshore Limited [1] 4C Offshore Limited [2]
X.	Gunfleet Sands Offshore Wind Farm (UK)	Siemens SWT-3.6-107 3.6 MW industrial offshore wind turbine	Sand and clay layers	Leblanc Thilsted and Tarp-Johansen [33] Lindoe Offshore Renewables Center [34]

designed to leap frog the rotational frequency range that would cause resonance of the structure due to the corresponding 3P frequency. For example, if the rotational speed range is 5–13 rpm, equivalent to 0.083–0.216 Hz, then the 3P frequency band is 0.25–0.65 Hz. If the structural natural frequency is 0.35 Hz, then the pitch control may regulate the rotational speed such that the corresponding 3P frequency avoids $\pm$ 10% of the structural natural frequency i.e. the frequency band 0.315–0.385 Hz to comply with the DNV code [25]. This would result in a jump in the rotational speed from 6.3 rpm to 7.7 rpm, avoiding operation between these values. Obviously, this is also not without cost, both in terms of initial costs, maintenance and power production.

The second issue is the top head mass, i.e. the mass of the rotor nacelle assembly (RNA, see Fig. 2 for clarity). With increasing capacity of the turbine, the mass of the rotor–nacelle assembly increases and the natural frequency will also decrease keeping other factors constant. Furthermore, the hub height is also higher due to longer blades (associated with heavier turbines) which increases the flexibility of the taller towers causing further reduction in the natural frequency. This trend can also be seen in Fig. 1, the target natural frequency of wind turbines (in soft–stiff design) with higher power output is typically lower. Fortunately, the large rotor diameter wind turbines also tend to have lower rotational speeds. This is because of the fact that for optimum power production the tip speed ratios (ratio of the speed of the tip of the blades and the incoming wind speed) are maintained at a favourable value, also to avoid blade damage. Furthermore, the top head mass is dependent on the choice of drive (with or without gearbox). Direct drive wind turbines do not need gearboxes, and thus significant weight reduction can be achieved (theoretically). However, the weight reduction is not obvious because the power of an electric generator is proportional to its rotational speed, see Eq. (1) [18] and thus direct drive wind turbines typically have larger diameter (and thus heavier) generators.

$$P = C_g D_g^2 L_g \Omega_g \tag{1}$$

where C_g is a constant and D_g, L_g, Ω_g are the diameter, length and rotational speed of the generator, respectively.

As the total mass of the rotor–nacelle assembly influences the natural frequency, the design of the support structure for wind turbines may be improved by an integrated design.

A further effect is the increasing importance of the flexibility of the monopile, the grouted connection and the transition piece (that is, the substructure) as a consequence of increasing water depth. The longer the monopile, the more effect the substructure has on the natural frequency of the total structure. This is in contrast with shallow water turbines where the tower is overwhelmingly softer than the substructure and the natural frequency of the whole system is critically governed by the bending stiffness of the tower and the soil stiffness.

For large wind turbines the frequency band of the wave excitation (see JONSWAP spectrum in Fig. 1) becomes important as it is very close to the natural frequency of the whole system. This issue gains even more importance as the substructure diameter increases for large wind turbines. If the structure is also installed in deeper water, then both the expected significant wave height and the length of the substructure increase, resulting in dynamic wave loads comparable to or exceeding the wind load.

The natural frequency of the whole system therefore needs to be assessed in the feasibility study phase and also in the early phases of the foundation design. This calls for a simplified methodology that is quick and uses only limited data about the wind turbine and the site.

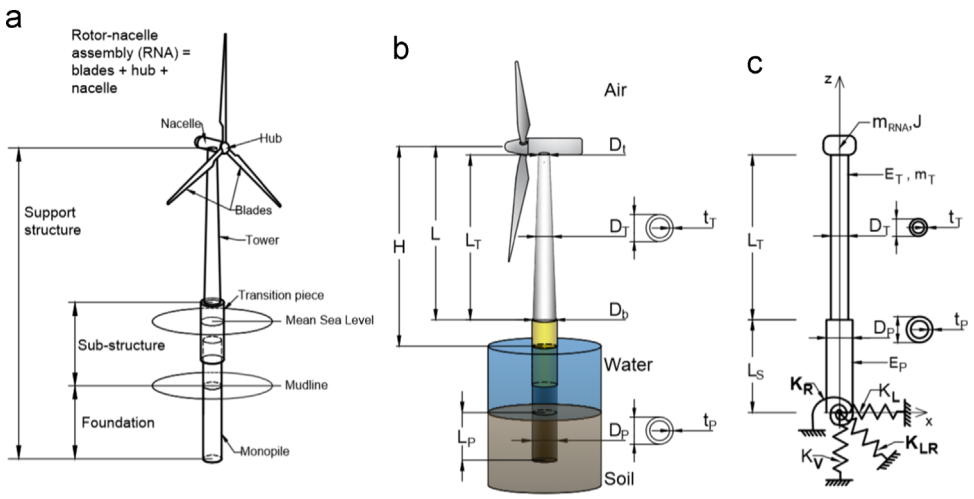

Fig. 2. Basic model of an OWT: (a) Main components. (b) Dimensions. (c) Mathematical model.

1.2. Motivation behind the study

This study aims to provide a simple, quick and reliable tool for the foundation designer to assess the fundamental natural frequency of the turbine-substructure-foundation-soil system. The simple expressions obtained in this work build on previous research in the dynamics of offshore wind turbines. Analysis of OWTs modelled as Euler–Bernoulli beams and founded on two independent springs (lateral and rocking stiffness) is carried out in [4,3] while soil–structure interaction was experimentally verified in [10]. A major discrepancy between measured and predicted natural frequencies of OWT structures has been reported in a multitude of studies [21,28,32,36,54,56]. The sources of uncertainty related to the discrepancy can be due to theory or physical idealisation of the system or parameters or a combination of the above and are summarised below:

(1) Beam model uncertainty i.e. uncertainty in the mathematical idealisation of the physical system: The current methodology is based on the Euler–Bernoulli beam theory, however, the authors have found in [6] that more sophisticated beam models including rotary inertia (Rayleigh beam) and shear deformation (Timoshenko beam) do not provide notable improvements in the results (less than 0.1%). Therefore, the simple Euler–Bernoulli model is satisfactory for wind turbine towers. Further details are given in Appendix A.
(2) Uncertainty in the modelling of the substructure: The substructure is modelled by a single equivalent cross section (which is the cross section of the monopile). This approximation may lead to over or underestimation of substructure stiffness.
(3) Uncertainty in the modelling of the foundation. The analysis focuses on Eigen solutions of a linear system, and therefore nonlinear soil behaviour is not modelled. The foundation system is not expected to go into the nonlinear regime and therefore the linear approximation is considered acceptable. In the linear regime, the foundation is modelled with three coupled springs (K_L, K_R and K_{LR}) resulting in an exact model of the linearised system, see Fig. 2(c). It was found in [6] that the cross coupling spring (K_{LR}) cannot be excluded from the analysis.
(4) The major uncertainty is the well-known issue of measurement of soil stiffness. It is challenging to estimate foundation stiffness with complex soil layers at offshore sites. A sensitivity analysis was carried out [7] and it was found that underestimation of soil stiffness by 30% would typically result in a frequency increase of 0.2–5% while overestimation by 30% causes a natural frequency change of 2–5.6%. The uncertainty analysis was carried out by considering the effect of stiffness changes for the ten wind turbines presented in Table 1, as well as 6 other industrial wind turbines not discussed in this paper. The transcendental equations resulting from the analytical formulation have been solved, using the three springs approximation for the foundation and Timoshenko beam theory for the tower, as given in Appendix B, and also in [6] (a simplified version of the problem has also been given in [4,3]). The equations have been numerically solved for all wind turbines in different soil conditions to analyse the sensitivity.
(5) Another aspect is the idealisation of the tapered tower of varying wall thickness with an equivalent diameter and wall thickness as a constant bending stiffness column, as has been used in many of the simplified methods [3,4,50,55,56,6].
(6) A further source of uncertainty is the damping of the real structure. If the damping ratio is ζ, the natural frequency of underdamped vibrations $\tilde{f}_1$ can be expressed with the undamped frequency f_1 as

$$\tilde{f}_1 = f_1\sqrt{1-\zeta^2}$$

The main sources of damping of an offshore wind turbine structure are the aerodynamic damping, soil damping, structural damping (damping of steel), hydrodynamic damping and additional damping from tower motion dampers (e.g. slosh dampers).

$$\zeta_{total} = \zeta_{aero} + \zeta_{struct.} + \zeta_{soil} + \zeta_{hydro.} + \zeta_{damper}$$

1.3. Damping of structural vibrations of offshore wind turbines

As the natural frequencies of offshore wind turbines are close to forcing frequencies, damping is critical to restrict damage accumulation and avoid premature maintenance. Therefore discussion is warranted for issues related to damping and for practical design purposes can be idealised in fore–aft and side-to-side vibrations of offshore wind turbines. The main difference between the sway-bending (or rocking) vibrations about two axes (X and Y in Fig. 2) is that in the along-wind direction higher damping is expected due to the high aerodynamic damping caused by the rotating blades interacting with the airflow. On the other hand, for the side-to-side direction, the aerodynamic damping is orders of magnitudes lower.

A non-operational (parked or idling) OWT has similar aerodynamic damping in the fore–aft as in the side-to-side direction.

Since the wind load is acting in the along-wind direction, the highest load amplitudes are expected in fore–aft motion. This is because for most wind turbines in water depths less than 30 m, wind loading is the dominant load, while for very large diameter monopiles in medium to deep water, wave loading is expected to have equal or higher magnitude. It is worth noting that due to the yaw mechanism of the wind turbine, the along-wind and cross-wind directions are dynamically moving and are not fixed, therefore the foundation is subjected to both cross-wind and along-wind loading in all directions during the lifetime of the OWT. One can conclude that analysing vibrations in both directions is important.

Studies considering the damping of the first bending mode either empirically or theoretically include Camp et al. [19], Tarpjohansen et al. [48], Versteijlen et al. [51], Damgaard and Andersen [21], Damgaard et al. [22] and Shirzadeh et al. [46]. Based on these studies and other estimates and in the absence of other data, the following assessment of damping ratio contributions is recommended:

- Structural damping: 0.15–1.5%. The value of structural damping depends on the connections in the structure (such as welded connections, grouted connections, etc.) in addition to material damping (usually steel) through energy dissipation in the form of heat (hysteretic damping).
- Soil damping: 0.444–1%. The sources of damping resulting from soil–structure interaction (SSI) include hysteretic (material) damping of the soil, wave radiation damping (geometric dissipation) and, to a much lesser extent, pore fluid induced damping. Wave radiation damping and pore fluid induced damping are negligible for excitations below 1 Hz, and therefore hysteretic damping is dominant for the purposes of this study. The soil damping depends on the type of soil and the strain level.
- Hydrodynamic damping: 0.07–0.23%. Results from wave radiation and viscous damping due to hydrodynamic drag. In the low frequency vibration of wind turbines the relative velocity of the substructure is low and therefore viscous damping, which is proportional to the square of the velocity is typically very low. The larger contribution results from wave radiation damping, which is proportional to the relative velocity.
- Aerodynamic damping: in the fore–aft direction for an operational turbine 1–6%, for a parking turbine or in the crosswind direction 0.06–0.23%. Aerodynamic damping is the result of the relative velocity between the wind turbine structure and the surrounding air. Aerodynamic damping depends on the particular wind turbine, and is inherent in the popular Blade Element Momentum (BEM) theory for aeroelastic analysis of wind turbine rotors. The magnitude for a particular wind turbine also depends on the rotational speed of the turbine.

The total damping of the first mode of vibration is typically between 1% and 4% in side-to-side vibration, or for a parked, stopped or idling turbine. On the other hand, the total damping is between 2% and 8% for an operational wind turbine in the fore–aft direction.

2. Methodology and results

In this study, the OWT mechanical model used in [4,3,6] is extended to consider the effect of the stiffness of the substructure which becomes critical for deeper water, see Fig. 2. The rotor–nacelle assembly (RNA) is modelled as a lumped top head mass m_{RNA} and the tower and the substructure are modelled as beams. The foundation is idealised as three springs (lateral K_L, rocking or rotational K_R, and cross coupling K_{LR} stiffness). This methodology requires 14 input parameters which are given in Table 1 and the definitions are shown in Fig. 2. Arany et al. [6] demonstrated that the more sophisticated Timoshenko beam model, which takes into account mass moment of inertia and shear deformation in the equations of motion of the tower, provides no notable improvement over the simpler Euler–Bernoulli beam model in natural frequency estimation. It was concluded that the tower can be considered a slender beam and the Euler–Bernoulli beam is sufficiently accurate, therefore it was used to obtain the results presented in this paper.

Appendix B shows the derivation of the frequency equations of the two beam models. The natural frequency in both cases can be obtained numerically from the resulting transcendental equations. Approximate closed form expressions have been fitted to the results to fit the expression given by Eq. (2) which states that the first natural frequency (f_1) can be obtained by multiplying the fixed base frequency (cantilever beam frequency f_{FB}) by two factors C_R and C_L which account for the flexibility provided by the foundation. In other words, the foundation flexibility coefficients C_R and C_L are applied to the fixed base (cantilever beam) natural frequency to obtain the natural frequency taking into account the foundation compliance and soil–structure interaction. The formula for the first mode natural frequency is then given as:

$$f_1 = C_R C_L f_{FB}. \tag{2}$$

2.1. Parameters and idealisation

The methodology uses 14 basic parameters for the wind turbine support structure and the site (foundation stiffness) and are summarised in Table 2. It is considered useful to explain the idealisation of the structure in a bit more detail. Fig. 2(b) shows the dimensions of the tapered and equivalent towers. The tapering is assumed to be linear with the tower diameter linearly decreasing from D_b at the bottom to D_t at the top of the tower. The average diameter is used as the equivalent constant diameter for the idealised tower D_T, that is

$$D_T = \frac{D_b + D_t}{2} \tag{3}$$

The wall thickness t_T is assumed to be constant along the tower. The equivalent mass of the tower is calculated from the geometry and density of the tower material ρ_T as

$$m'_T = \rho_T D_T \pi t_T L_T \tag{4}$$

Table 2
Information required for frequency estimation.

#	Input parameter	Symbol	Unit
1	Mass of the rotor–nacelle assembly	m_{RNA}	ton
2	Tower height	L_T	m
3	Tower top diameter	D_t	m
4	Tower bottom diameter	D_b	m
5	Average tower wall thickness	t_T	m
6	Tower Young's modulus	E_T	GPa
7	Tower mass	m_T	ton
8	Platform height above mudline	L_S	m
9	Monopile diameter	D_P	m
10	Monopile wall thickness	t_P	m
11	Monopile Young's modulus	E_P	GPa
12	Lateral stiffness of foundation	K_L	GN/m
13	Cross stiffness of foundation	K_{LR}	GN
14	Rocking stiffness of foundation	K_R	GN m/rad

Note, in some cases this mass may not necessarily be exactly the same as the actual mass of the tower m_T. However, in cases when the average tower thickness or a range of tower wall thicknesses is not available, the thickness can be back-calculated from the tower mass

$$t_T' = \frac{m_T}{\rho_T L_T D_T \pi} \tag{5}$$

The model is based on a beam with two different cross section. It is assumed that the cross section of the monopile is the first section of the beam from the mudline to the bottom of the tower, and the second section of the beam is the tower from the tower bottom to the rotor nacelle assembly. In this formulation the flexibilities of the grouted connection and the transition piece are neglected. The first section is of length L_S, diameter D_P, wall thickness t_P and bending stiffness $E_P I_P$, while the second cross section is of length L_T, diameter D_T, wall thickness t_T and bending stiffness $E_T I_T$. The platform height above mudline L_S is defined as the distance from the mudline (seabed) to the bottom of the tower (tower – transition piece connection).

2.2. Calculation procedure for simple natural frequency estimation

The natural frequency estimation process can be summarised in three steps:

Step 1: Calculate fixed base natural frequency f_{FB} of the variable cross section beam using the monopile flexibility coefficient C_{MP}.
Step 2: Calculate the non-dimensional foundation stiffness parameters: $\eta_L, \eta_R, \eta_{LR}$.
Step 3: Calculate and apply foundation flexibility coefficients C_L and C_R and apply them to obtain the first natural frequency on the flexible foundation, i.e. $f_1 = C_L C_R f_{FB}$

The steps are described in more detail along with the methodology and calculation steps together with references for further reading.

Calculation procedure for Step 1: The fixed base natural frequency can be calculated by the simple natural frequency formula of the cantilever beam. The derivation can be found in Appendix A.

$$f_{FB} = \frac{1}{2\pi}\sqrt{\frac{k}{m}} \tag{6}$$

where for the tower and the RNA only, the equivalent stiffness of the beam k based on the tower bending stiffness $E_T I_T$ and length L_T, and the equivalent mass (considering the mass of the tower m_T' and the mass of the rotor–nacelle assembly m_{RNA}) are given by:

$$k = \frac{3E_T I_T}{L_T^3} \quad \text{and} \quad m = m_{RNA} + \frac{33}{140} m_T' \tag{7}$$

Substituting back into the formula, the following is given for the fixed base natural frequency.

$$f_{FB,T} = \frac{1}{2\pi}\sqrt{\frac{3E_T I_T}{L^3\left(m_{RNA} + \frac{33}{140} m_T'\right)}} \tag{8}$$

In these expressions the second moment of area I_T and the mass m_T' of a constant diameter tower are considered. That is, if the average diameter of the tower is D_T and the average wall thickness of the tower is t_T then the equivalent second moment of area I_T and the equivalent tower mass m_T' are

$$I_T = \frac{1}{8}\pi D_T^3 t_T \quad m_T' = \rho_T D_T \pi t_T L_T \tag{9}$$

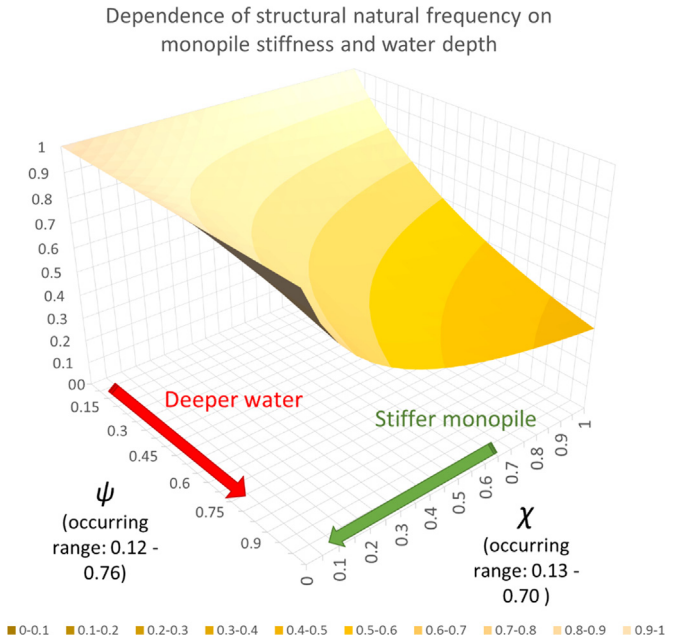

Fig. 3. The effect of water depth and monopile stiffness on the fixed base natural frequency.

A similar expression is given specifically for wind turbine towers by van der Tempel and Molenaar [50].

$$f_{FB,T} = \frac{1}{2\pi}\sqrt{\frac{3.04E_T I_T}{L^3\left(m_{RNA} + 0.227 m_T'\right)}} \tag{10}$$

In this paper the simple expression in Eq. (8) is used. The flexibility of the monopile is taken into account by a monopile flexibility coefficient C_{MP} expressed in terms of two non-dimensional numbers,

$$\text{bending stiffness ratio}: \quad \chi = \frac{E_T I_T}{E_P I_P}$$

$$\text{platform/tower length ratio}: \quad \psi = \frac{L_S}{L_T}.$$

where $E_T I_T$ is the bending stiffness of the constant diameter tower, $E_P I_P$ is the bending stiffness of the monopile, L_S is the platform height above the seabed (distance from the mudline to the top of the transition piece) and L_T is the height of the tower.

The fixed base natural frequency of the wind turbine – substructure system is

$$f_{FB} = C_{MP} \cdot f_{FB,T} = \sqrt{\frac{1}{1 + (1+\psi)^3 \chi - \chi}} f_{FB,T} \tag{11}$$

Fig. 3 shows the effect of the parameters χ and ψ on the fixed base natural frequency. To make these parameters more physically meaningful, one can say that increasing χ represents a stiffer monopile, while increasing ψ represents deeper water.

Calculation procedure for Step 2: In the second step, the foundation stiffness is non-dimensionalised using the tower's length L_T and the equivalent bending stiffness of the tapered tower EI_η. The non-dimensional lateral, cross-coupling and rotational stiffness values, $\eta_L, \eta_{LR}, \eta_R$ respectively, are necessary for this calculation

$$\eta_L = \frac{K_L L_T^3}{EI_\eta} \qquad \eta_{LR} = \frac{K_{LR} L_T^2}{EI_\eta} \qquad \eta_R = \frac{K_R L_T}{EI_\eta} \tag{12}$$

These formulae use the equivalent bending stiffness for a tapered tower as given in [7–9]. The derivation is shown in

Appendix C. Only the final formulae are presented here for brevity:

$$EI_\eta = EI_t \times f(q) \tag{13}$$

where EI_t is the bending stiffness at the top of the tower.

$$f(q) = \frac{1}{3} \times \frac{2q^2(q-1)^3}{2q^2 \ln q - 3q^2 + 4q - 1} \quad \text{with} \quad q = \frac{D_b}{D_t} \tag{14}$$

Calculation procedure for Step 3: The empirical foundation flexibility factors are applied to the natural frequency

$$C_R(\eta_L, \eta_R, \eta_{LR}) = 1 - \frac{1}{1 + a\left(\eta_R - \frac{\eta_{LR}^2}{\eta_L}\right)}$$
$$C_L(\eta_L, \eta_R, \eta_{LR}) = 1 - \frac{1}{1 + b\left(\eta_L - \frac{\eta_{LR}^2}{\eta_R}\right)} \tag{15}$$

where a, b are empirical constants. The values of these constants were found to be $a \approx 0.6$ and $b \approx 0.5$ and were obtained by fitting closed form curves to the solutions obtained by solving the transcendental equations resulting from the analytical formulation given in Appendix B. Further details can be found in [6] and a simplified version of the problem has also been solved in [4,3]. A total of 16 wind turbines have been used to find best-fit values of a and b minimising the mean squared error between the numerical and closed form results. The curve fit reproduces the natural frequency for all 16 wind turbines with excellent accuracy ($< 1\%$) for practical parameter combinations. The applicability of the formulae in Eq. (15) is limited to

$$\eta_R > 1.2\frac{\eta_{LR}^2}{\eta_L} \quad \text{and} \quad \eta_L > 1.2\frac{\eta_{LR}^2}{\eta_R} \tag{16}$$

With these the natural frequency of the OWT on a flexible foundation can be calculated as given in Eq. (2).

2.3. Example step by step calculation: Blyth Offshore Wind Farm Vestas V66 2 MW

The input data for the calculations are shown in Table 3 (number III). Foundation stiffness is one of the most uncertain quantities and Appendix D discusses a method to obtain foundation stiffness in the absence of detailed site data.

Step 1: The parameters in Table 2 are used to calculate the fixed base natural frequency of the tower

$$f_{FB,T} = \frac{1}{2\pi}\sqrt{\frac{3E_T I_T}{(m_{RNA} + \frac{33}{140}m_T')L^3}} = 0.703[\text{Hz}] \tag{17}$$

In this formulation D_T is the average tower diameter

$$D_T = \frac{D_b + D_t}{2} = \frac{4.25 + 2.75}{2} = 3.5[\text{m}], \tag{18}$$

The tower wall thickness is determined from the mass of the tower as

$$t_T = \frac{m_T}{\rho_T D_T \pi L_T} = \frac{159,000[\text{kg}]}{7860[\text{kg/m}^3] \cdot 3.5[\text{m}] \cdot \pi \cdot 55[\text{m}]} \approx 0.034[\text{m}] \tag{19}$$

and I_T is the second moment of area of the equivalent constant diameter tower cross section

$$I_T = \frac{1}{8}D_T^3 t_T \pi = \frac{1}{8} \cdot 3.5^3[\text{m}^3] \cdot 0.034[\text{m}] \cdot \pi = 0.572[\text{m}^4]. \tag{20}$$

The bending stiffness ratio and length ratio are calculated as

$$\chi = \frac{E_T I_T}{E_P I_P} = \frac{210[\text{GPa}] \cdot 0.572[\text{m}^4]}{210[\text{GPa}] \cdot 0.806[\text{m}^4]} = 0.710[-] \tag{21}$$

$$\psi = \frac{L_S}{L_T} = \frac{16[\text{m}]}{55[\text{m}]} = 0.306[-] \tag{22}$$

where the monopile's second moment of area is

$$I_P = \frac{1}{8}D_P^3 t_P \pi = \frac{1}{8} \cdot 3.5^3 \cdot 0.05 \cdot \pi = 0.806[\text{m}^4]. \tag{23}$$

The natural frequency of the monopile supported wind turbine on a fixed base is given as

$$f_{FB} = C_{MP} \cdot f_{FB,T} = \sqrt{\frac{1}{1 + (1 + 0.306)^3 \cdot 0.710 - 0.710)}} \cdot 0.703[\text{Hz}] = 0.514[\text{Hz}] \tag{24}$$

Step 2: The equivalent bending stiffness needed for the non-dimensional stiffness parameters is calculated.

$$q = \frac{D_b}{D_t} = \frac{4.25}{2.75} = 1.55 \qquad f(q) = \frac{1}{3} \times \frac{2q^2(q-1)^3}{2q^2 \ln q - 3q^2 + 4q - 1} = 2.69 \tag{25}$$

$$EI_\eta = EI_{\text{top}} \times f(q) \approx 147[\text{GNm}^2] \tag{26}$$

See details on the derivation of these expressions in Appendix B. Then the non-dimensional stiffness parameters can be obtained from

$$\eta_L = \frac{K_L L^3}{EI_\eta} = 45709[-] \tag{27}$$

Table 3
Input parameters for wind turbines listed in Table 1.

#	Input parameter	Symbol	Unit	I	II	III	IV	V	VI	VII	VIII	IX	X
1	Mass of the rotor–nacelle assembly	m_{RNA}	ton	32	35.7	80	130.8	130.8	130.8	130.8	234.5	234.5	234.5
2	Tower height	L_T	m	37.9	44.5	54.5	60.06	58	54.1	53	66	67.3	60
3	Tower bottom diameter	D_b	m	3.2	3.5	4.25	4.45	4.45	4.3	4.3	5	5	5
4	Tower top diameter	D_t	m	1.9	1.7	2.75	2.3	2.3	2.3	2.3	3	3	3
5	Average tower wall thickness	t_T	mm	13	13	34	22	32	36	28	28	41	33
6	Tower Young's modulus	E_T	GPa	210	210	210	210	210	210	210	210	210	210
7	Tower weight	m_T	ton	31.44	37	159	108	153	160	120	180	260	193
8	Platform height above mudline	L_S	m	7.1, 12.1	5.2–6.0	16.5	16	33	41.1	37	22.8	37.3	28
9	Monopile diameter	D_P	m	3.2, 3.7	3.515	3.5	4.3	4.75	4.7	5	4.7	6	5
10	Monopile wall thickness	t_P	mm	35	35	5	45	45–80	65	50–75	45–75	80	35–50
10	Monopile Young's modulus	E_P	GPa	210	210	210	210	210	210	210	210	210	210
11	Lateral stiffness of foundation	K_L	GN/m	0.52, 0.62	0.58	42.66	0.82	1.03	1.05	1.02	1.11	1.53	1.02
12	Cross stiffness of foundation	K_{LR}	GN	−2.74, −3.57	−3.25	−45.50	−5.42	−7.68	−7.89	−7.59	−8.56	−13.88	−7.59
13	Rocking stiffness of foundation	K_R	GN m/rad	23.63, 33.59	29.67	136.04	58.77	93.45	96.84	91.93	108.03	205.72	91.93

$$\eta_{LR} = \frac{K_{LR}L^2}{EI_\eta} = -903[-] \tag{28}$$

$$\eta_R = \frac{K_R L}{EI_\eta} = 50[-] \tag{29}$$

Step 3: The foundation flexibility factors are calculated

$$C_R(\eta_L, \eta_R, \eta_{LR}) = 1 - \frac{1}{1 + 0.6\left(50 - \frac{(-903)^2}{45709}\right)} = 0.951 \tag{30}$$

$$C_L(\eta_L, \eta_R, \eta_{LR}) = 1 - \frac{1}{1 + 0.5\left(45709 - \frac{(-903)^2}{50}\right)} = 1.000 \tag{31}$$

the natural frequency is then obtained from

$$f_1 = C_R C_L f_{FB} = 0.951 \cdot 1.000 \cdot 0.514[\text{Hz}] = 0.489[\text{Hz}] \tag{32}$$

The measured frequency at Blyth wind farm is 0.488 Hz, and thus there is an excellent match with an error of 0.2%. The natural frequency on the monopile foundation is about 4.9% lower than it would be on a completely stiff fixed base. This difference is small because at the Blyth site the monopile is grouted into very stiff bedrock. The influence of the foundation flexibility is higher for most sites with values ranging from 4% to 15% for wind turbines analysed in this paper.

3. Application of the methodology to installed wind turbines and discussion

To demonstrate the general applicability of this method, the natural frequency of several wind turbines will be determined. The analysed offshore wind farms and turbines are presented in Table 1, as well as references to the sources of data. The input data of the turbines is summarised in Table 2. The calculations shown in Section 2.3 are carried out for all wind turbines in Table 1. Some intermediate parameters are shown in Table 4 and the results are given in Table 5 and compared with the measured data. The measured natural frequency values have been reported by various researchers and have been obtained by different methodologies of signal processing. Further details on the case studies can be found in the references given in Table 1. The results show that the empirical formula presented in this paper approximates the natural frequency within −3.2% to 3.1% of the measured frequency. This can be considered an excellent match given such a simplified methodology. The difference between the fixed base natural frequency and that for the flexible foundation using the present method is typically within the range 3–15%, which is considered typical for most offshore wind turbines. The flexibility (percentage reduction of the first natural frequency) introduced by the compliance of the foundation is reported for each wind turbine in Table 5.

As the foundation stiffness parameter (K_L, K_R) increases, the foundation flexibility coefficients (C_L, C_R) also increase and the natural frequency approaches the fixed base natural frequency f_{FB}. Most of the contribution to the frequency change (4–15%) results from the rotational foundation flexibility coefficient C_R and the lateral foundation stiffness coefficient C_L has very limited influence (of less than 1% on the natural frequency) of all analysed turbines. Consequently, the most important foundation stiffness parameter is the rotational stiffness K_R.

In Fig. 4 three turbines are used to illustrate the effect of the non-dimensional rotational stiffness η_R on the natural frequency in terms of the rotational foundation flexibility coefficient C_R. It should be noted that the curves flatten out for increasing rotational stiffness. The foundation designer should choose the foundation stiffness such that the OWT structure is in the flat part of this curve. This ensures that even if the foundation stiffness was estimated with significant errors or if the stiffness changes during the lifetime of the turbine, the natural frequency change is limited and does not affect the foundation's ability to meet the Fatigue Limit State (FLS) and Serviceability Limit State (SLS) criteria. On the dropping part of the curve, however, a slight increase or decrease of the stiffness might cause substantial change in the natural frequency, which may lead to increased fatigue damage and reduced service life.

It is important to emphasise that the foundation stiffnesses K_L, K_{LR}, K_R and thus the non-dimensional foundation stiffnesses η_L, η_{LR}, η_R are not independent parameters. Appendix D provides a brief discussion about the available methods for estimating the foundation stiffness, and simple expressions are provided for the simple cases of cohesive soils, cohesionless soils and rock. Following these formulae, the independent parameters of foundation stiffness are the geometry of the pile (diameter D_P, wall thickness t_P and embedded length L_P as defined in Fig. 2(b)) and soil parameters (expressed using either the modulus of subgrade reaction k_h, the coefficient of subgrade reaction n_h or the effective shear modulus G^*).

Furthermore, as discussed in Section 1, the damping in the first sway-bending mode also influences the measured natural frequency. The damping is lower for side-to-side direction and for a parked/idling turbine than in the fore–aft direction for an operational turbine due to the significant contribution of aerodynamic damping. The total damping of the system was estimated between 2% and 8% in Section 1, which amounts to a frequency change of about 0.02–0.32%.

3.1. Discussion on the parameters for foundation stiffness estimation

There are two groups of parameters necessary to determine foundation stiffness, categorised as pile data and soil data, as tabulated in Tables 6 and 7 for all the turbines listed in Table 1. The pile parameters are the pile diameter D_P, the pile wall thickness t_P, and the pile embedded length L_P, as defined in Fig. 2(b). The diameter of monopiles is typically constant along the length. However, the pile wall thickness may change. In this paper the wall thickness was chosen as the pile thickness in the region below the mudline, because the top layers are considered more

Table 4
Calculated parameters for wind turbines listed in Table 1.

Parameter	Symbol	Unit	I	II	III	IV	V	VI	VII	VIII	IX	X
Tower average diameter	D_T	m	2.55	2.6	3.5	3.375	3.375	3.3	3.3	4	4	4
Average second moment of area	I_T	m^4	0.086	0.089	0.574	0.325	0.478	0.512	0.392	0.694	1.034	0.818
Tower diameter ratio D_b/D_t	q	Dimensionless	1.68	2.06	1.55	1.935	1.935	1.870	1.870	1.667	1.667	1.667
Bending stiffness coefficient for η	$f(q)$	Dimensionless	3.28	5.23	2.02	4.528	4.528	4.181	4.181	3.204	3.204	3.465
Equivalent bending stiffness of the tapered tower for non-dimensional stiffness parameters	EI_η	GN m^2	21.86	16.73	116.71	92.8	66.8	61.7	61.7	173.9	267.5	136.5

Table 5
Natural frequency results.

Wind farm	Turbine ID	Natural frequency [Hz]			**Error [%]**	Flexibility [%]
		Measured	Fixed base	Formula		
I. Lely	A2	0.634	0.713	0.643	**1.36**	9.9
	A3	0.735	0.767	0.712	**−3.19**	7.2
II. Irene Vorrink	3	0.546	0.583–0.586	0.552–0.555	**−1.10**	5.3
	7	0.554			**−0.18**	5.8
	12	0.553			**0.18**	5.3
	23	0.563			**1.42**	5.8
	28	0.560			**0.89**	5.8
III. Blyth	Southernmost	0.488	0.514	0.489	**0.12**	4.9
IV. Kentish Flats	–	0.339	0.380	0.339	**0.01**	10.9
V. Barrow	–	0.369	0.387	0.367	**0.54**	5.2
VI. Thanet	–	0.370	0.402	0.382	**3.08**	5.0
VII. Belwind	–	0.372	0.401	0.380	**2.12**	5.4
VIII. Burbo Bank	–	0.292	0.322	0.295	**1.05**	8.4
IX. Walney	–	0.350	0.380	0.349	**0.40**	8.4
X. Gunfleet Sands	–	0.314	0.352	0.315	**0.31**	10.6

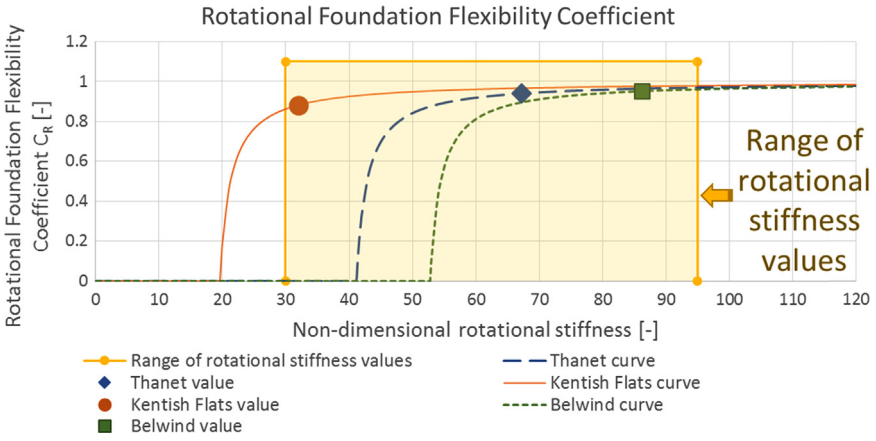

Fig. 4. Rotational foundation flexibility coefficient curves as a function of non-dimensional rotational stiffness for three different sites, all using Vestas V90 3 MW offshore wind turbines.

Table 6
Input and calculated soil parameters for each wind turbine listed in Table 1.

#	**Input parameter**	**Symbol**	**Unit**	**I**	**II**	**III**	**IV**	**V**	**VI**	**VII**	**VIII**	**IX**	**X**
1	Soil density	ρ_S	kg/m^2	2000	2000	2850	920	920	920	920	2090	2000	2000
2	Soil's Young's modulus	E_S	MPa			5160							
3	Soil's Poisson's ratio	ν	Dimensionless			0.2							
4	Soil's shear modulus	G_S	MPa			2150.0							
	Soil coefficient of subgrade reaction	n_h	MN/m^3	29.1	29.1		6.2	6.2	6.2	6.2	30.4	29.1	29.1
	Soil's equivalent shear modulus	G^*	MPa			2472.50							

Table 7
Input and calculated pile parameters for each wind turbine listed in Table 1.

#	**Input parameter**	**Symbol**	**Unit**	**I**	**II**	**III**	**IV**	**V**	**VI**	**VII**	**VIII**	**IX**	**X**
1	Pile diameter (range)		m	3.2–3.7	3.515	3.5	4.3	4.75	4.05–5.1	4.07–5.0	4.7	6	4.7
	Chosen value	D_P	m	3.2; 3.7	3.515	3.5	4.3	4.75	4.7	5	4.7	6	4.7
2	Pile wall thickness (range)		mm	35	35	50	35–50	45–80	60	50–75	45–75	80	50–94
	Chosen value	t_P	mm	35	35	50	45	80	60	70	75	80	94
3	Pile embedded length (range)		m	30	23–24.6	12–15	18–34	30.2–40.7	25–30	35	21–24	30	27–38
	Chosen value	L_P	m	30	24.6	15	29.5	40	30	35	24	30	38
4	Pile material's Young's modulus	E_P	GPa	210	210	210	210	210	210	210	210	210	210
	Pile equivalent Young's modulus	E_e	GPa	15.45	16.23	22.99	17.04	26.89	20.64	22.55	25.55	21.52	31.62
	Pile bending stiffness	$E_P I_P$	GN m^2	142.09	121.64	169.32	285.88	671.92	494.29	691.70	611.89	1368.78	757.49
	Pile slenderness parameter	βL_P	Dimensionless	2.712	2.310	4.459	2.750	3.329	2.711	3.138	1.931	1.529	2.338

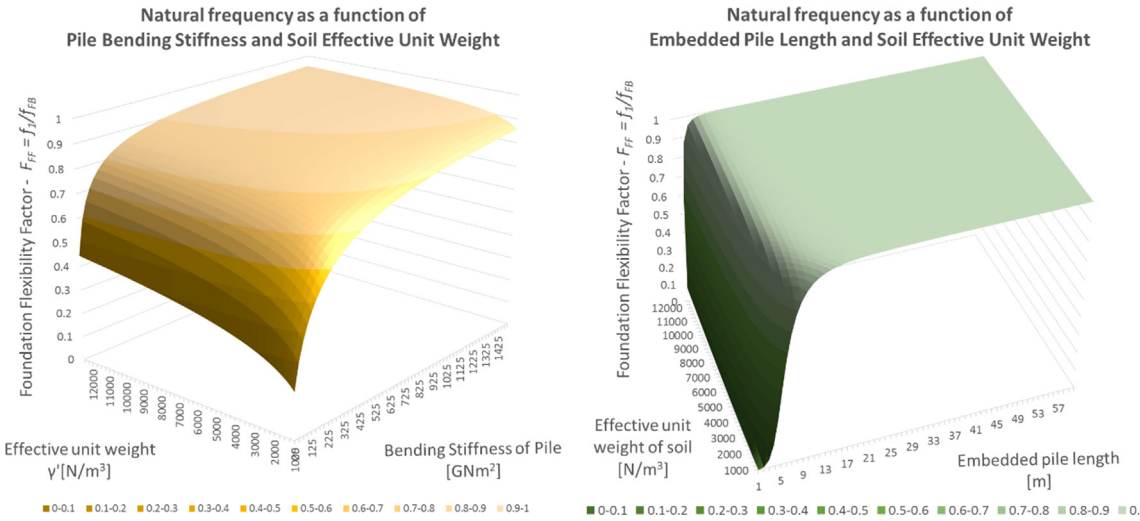

Fig. 5. Foundation flexibility factor as a function of soil effective unit weight and pile bending stiffness for slender piles and as a function of soil effective unit weight and embedded length for rigid piles.

important from the point of view of pile head deflection/rotation and pile stiffness. As can be seen based on Appendix D, the stiffness of the soil is described by different parameters for different soil types. For cohesive soils where the modulus of subgrade reaction is considered constant with depth below mudline, the critical parameter is the modulus of subgrade reaction k_h. For cohesionless soils where k_h increases linearly with depth, the key parameter is the coefficient of subgrade reaction n_h, which describes the rate at which the modulus of subgrade reaction increases with depth. The parameter n_h, however, is a simple linear function of the unit weight γ_S and thus the density ρ_S of the cohesionless soil using the formula of Terzaghi [49] as given in Eq. (D5) (in Appendix D). In case of rocks the important parameters are the shear modulus G_S and the Poisson's ratio ν_S, from which the effective shear modulus of Eq. (D7) can be calculated.

As mentioned in Section 3, the foundation stiffness parameters K_L, K_R and K_{LR} are not independent. It is apparent from Table D1 (in Appendix D) that the independent parameters required to determine the foundation flexibility factor $F_{FF} = C_R C_L$ are different for each soil type and pile slenderness combination. The simplest cases are for cohesionless soils where only two independent parameters are necessary. For slender piles these are the density of soil ρ_S and the bending stiffness of the monopile $E_P I_P$, and for rigid piles they are the soil density ρ_S and the pile embedded length L_P. These two cases are shown in Fig. 5. There are more independent parameters for clays and rock, and those cases therefore do not allow for easy visualisation.

4. Conclusions

A simple methodology has been presented to calculate the first natural frequency of an offshore wind turbine founded on a monopile. The methodology is based on multiplying the fixed base cantilever beam natural frequency by two foundation flexibility factors to include the compliance of the foundation as well as the flexibility of the substructure. The monopile foundation is modelled by three coupled springs (lateral, rotational and cross coupling stiffness). The closed form formulae presented in this paper were obtained from fitting curves to the natural frequency results obtained from numerically solving the transcendental equations. Several conclusions can be drawn from this study:

- It is shown through the study of 10 wind turbines that the natural frequency can be predicted with accurately (the error range is $\pm 3.5\%$).
- For the wind turbines considered, foundation flexibility reduced the fixed base natural frequency typically by 4–15%.
- The foundation flexibility factor is very sensitive to the rotational stiffness K_R of the monopile. On the other hand, the natural frequency change from the fixed base frequency due to lateral stiffness of the monopile (K_L) is limited to about 1%.
- The simple framework for the calculation of the foundation stiffness following the work of Poulos and Davis [42] Randolph [43] and Carter and Kulhawy [20] used in this study was found to give reasonable results for the 10 wind turbines studied where three different soil types (cohesive/clay, cohesionless/sand and rock) and two limit case approximations of slender/infinitely long and rigid/infinitely stiff piles were analysed. It was found that most real monopiles fall between the limiting cases of infinitely long and rigid piles.
- The effect of water depth and monopile stiffness were also analysed and it is found that the methodology can correctly represent the flexibility of the monopile and therefore the approximation is applicable both in shallow and deep water.
- While the final design verification can be carried out using detailed finite element investigations, the method presented in the paper can be used to estimate the natural frequency using limited information about the wind turbine and the site and may be a useful tool for initial analyses and conceptual design.

Acknowledgement

The first author is supported by an EPSRC DTP studentship via the University of Bristol.

Appendix A. – Natural frequency of a cantilever beam with variable cross section

The motion of the cantilever beam can be described as a single degree of freedom mass-spring system. The free vibration of this system is given by

$$m\ddot{x}(t) + kx(t) = 0 \tag{A1}$$

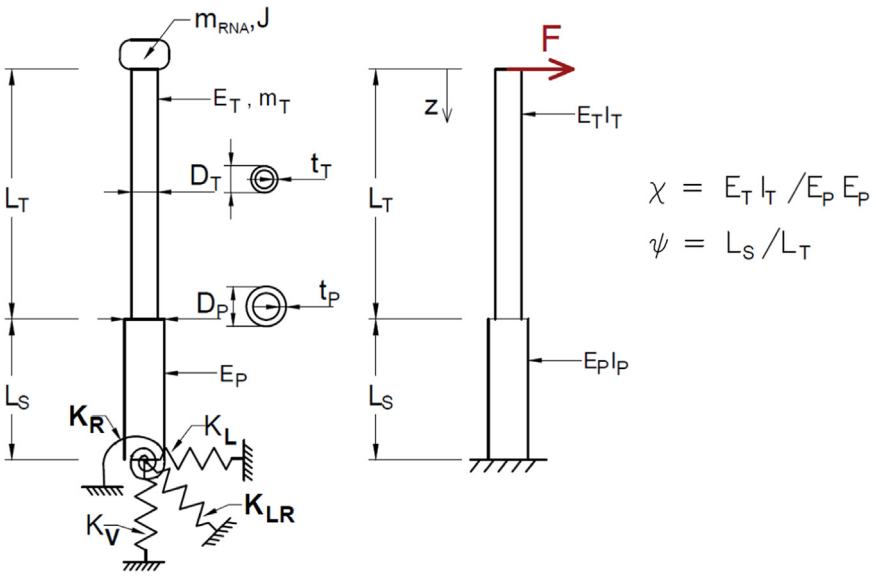

Fig. A1. Cantilever beam with variable cross section.

Table A1
Non-dimensional variables.

Dimensionless group	Formula	Dimensionless group	Formula
Non-dimensional lateral stiffness	$\eta_L = \frac{K_L L_T^3}{EI_\eta}$	Non-dimensional axial force	$\nu = \frac{P^* L_T^2}{EI_\nu}$
Non-dimensional rotational stiffness	$\eta_R = \frac{K_R L_T}{EI_\eta}$	Mass ratio	$\alpha = \frac{m_{RNA}}{m_T}$
Non-dimensional cross stiffness	$\eta_{LR} = \frac{K_{LR} L_T^2}{EI_\eta}$	Non-dimensional rotary inertia	$\beta = \frac{J}{\mu L^2}$

K_L, K_R, K_{LR} are the lateral, rotational and cross stiffness of the foundation, respectively; EI_η is the equivalent bending stiffness of the tapered tower; L_T is the hub height above the bottom of the tower; P^* is the modified axial force, m_{RNA} is the mass of the rotor–nacelle assembly; m_T is the mass of the tower; J is the rotary inertia of the top mass; μ is the equivalent mass per unit length of the tower.
*The rotary inertia is taken to be zero for all wind turbines considered as information is not available in the referenced literature.

Assuming harmonic vibration, the following equation can be obtained:

$$-m\omega^2 + k = 0 \quad \text{with} \quad k = \frac{3EI}{L_T^3} \quad \text{and} \quad m = m_{RNA} + \frac{33}{140} m'_{tower} \tag{A2}$$

and from the circular frequency the Hertz frequency is easily obtained

$$\omega = \sqrt{\frac{k}{m}} \quad \rightarrow \quad f_1 = \frac{1}{2\pi}\sqrt{\frac{k}{m}} \tag{A3}$$

The flexibility of the substructure expresses the dependence of the natural frequency on the water depth, that is, the flexibility of the monopile above the mudline and that of the transition piece. For the sake of simplicity, the model used in this paper assumes that the monopile's bending stiffness continues throughout the water depth and up to the root of the tower. For clarity, see Fig. A1.

$$\text{Bending stiffness ratio} : \chi = \frac{E_T I_T}{E_P I_P} \tag{A4}$$

$$\text{Platform/tower length ratio} : \psi = \frac{L_S}{L_T} \tag{A5}$$

Castigliano's second theorem for a linearly elastic 1 DoF structure can be written as

$$q = \frac{\partial U}{\partial Q}$$

where U is the strain energy, q is the generalised displacement, and Q is the generalised force. For the particular problem, the theorem can be used to calculate the top head deflection (the total deflection at the hub $w(0)$) due to a horizontal force F acting at the hub as

$$\begin{aligned} w(0) &= \frac{\partial U}{\partial F} = \frac{\partial}{\partial F}\int_0^{L_T+L_S} \frac{[M(z)]^2}{2EI(z)} dz = \frac{\partial}{\partial F}\int_0^{L_T} \frac{F^2 z^2}{2E_T I_T} dz \\ &+ \frac{\partial}{\partial F}\int_{L_T}^{L_T+L_S} \frac{F^2 z^2}{2E_P I_P} dz = \left[\frac{Fz^3}{3E_T I_T}\right]_0^{L_T} + \left[\frac{Fz^3}{3E_P I_P}\right]_{L_T}^{L_T+L_S} \\ &= \frac{FL_T^3}{3E_T I_T} + \frac{F(L_T+L_S)^3}{3E_P I_P} - \frac{FL_T^3}{3E_P I_P} \end{aligned} \tag{A6}$$

where the moment distribution along the structure caused by the horizontal force F is given as

$$M(z) = Fz \tag{A7}$$

The stiffness of the 1DoF system is then given as

$$\begin{aligned} k &= \frac{F}{w(0)} = \frac{1}{\frac{L_T^3}{3E_T I_T} + \frac{(L_T+L_S)^3}{3E_P I_P} - \frac{L_T^3}{3E_P I_P}} \\ &= \frac{3E_T I_T}{L_T^3 + \left(L_T^3 + 3L_T^2 L_S + 3L_T L_S^2 + L_S^3\right)\chi - L_T^3 \chi} = \frac{3E_T I_T}{L_T^3\left(1 + (1+\psi)^3 \chi - \chi\right)} \end{aligned} \tag{A8}$$

From this the natural frequency is calculated as

$$f_{FB} = \frac{1}{2\pi}\sqrt{\frac{k}{m}} \tag{A9}$$

where m is the generalised mass of the 1DoF system. The stiffness can be written as

$$k = \frac{1}{1+(1+\psi)^3\chi-\chi} k_T \tag{A10}$$

where k_T is the stiffness of the tower without the substructure, given as

$$k = \frac{3E_T I_T}{L_T^3}$$

The fixed-base natural frequency of the tower-substructure system (excluding foundation stiffness) is given using the bending stiffness ratio χ and the platform/tower length ratio ψ as

$$f_{FB} = \sqrt{\frac{1}{1+(1+\psi)^3\chi-\chi}} f_{FB,T} \tag{A11}$$

Appendix B. The Euler-Bernoulli beam model equation

The equation of motion using the Euler–Bernoulli beam model for a beam with an axial force is

$$\frac{\partial^2}{\partial z^2}\left(EI(z)\frac{\partial^2 w(z,t)}{\partial z^2}\right)+\mu(z)\frac{\partial^2 w(z,t)}{\partial t^2}+\frac{\partial}{\partial z}\left(P^*\frac{\partial w(z,t)}{\partial z}\right)=p(z,t) \tag{B1}$$

where $EI(z)$ is the bending stiffness distribution along the axial coordinate z, $\mu(z)$ is the distribution of mass per unit length, P^* is the axial force acting on the beam due to the top head mass and the self-weight of the tower, $p(z,t)$ is the excitation of the beam, $w(z,t)$ is the deflection profile.

Using constant equivalent values for the axial force, bending stiffness and mass per length, and considering free harmonic vibration of the beam with separation of variables $w(z,t)=W(z)\bullet e^{i\omega t}$, the equation can be reduced to the following using the non-dimensional parameters of Table A1 and the dimensionless axial coordinate $\xi = z/L$:

$$W''''+\nu W''-\Omega^2 W=0 \tag{B2}$$

where $\nu = P^* L_T^2/EI_\nu$ is the non-dimensional axial force and $\Omega = \omega/c_0 = \omega\sqrt{E_T I_T/m_T L^3}$ is the non-dimensional circular frequency.

Using the non-dimensional numbers as defined above, the boundary conditions can be written for the bottom of the tower ($\xi=0$):

$$W'''(0)+(\nu+\eta_{LR})W'(0)+\eta_L W(0)=0 \tag{B3}$$

$$W''(0)-\eta_R W'(0)+\eta_{LR} W(0)=0 \tag{B4}$$

and the top of the tower ($\xi=1$):

$$W'''(1)+\nu W'(1)+\alpha\Omega^2 W(1)=0 \tag{B5}$$

$$W''(1)-\beta\Omega^2 W'(1)=0 \tag{B6}$$

The parameters used in the boundary conditions are defined in Table A1. The characteristic equation for the equation of motion can be written as

$$\lambda^4+\nu\lambda^2-\Omega^2=0 \text{ or } \tilde{z}^2+\nu\tilde{z}-\Omega^2=0 \text{ with } \tilde{z}=\lambda^2 \tag{B7}$$

and

$$\tilde{z}_{1,2}=\frac{-\nu\pm\sqrt{\nu^2+4\Omega^2}}{2}=-\frac{\nu}{2}-\sqrt{\left(\frac{\nu}{2}\right)^2+\Omega^2},-\frac{\nu}{2}+\sqrt{\left(\frac{\nu}{2}\right)^2+\Omega^2}$$

The four solutions are then

$$r_1=i\sqrt{\tilde{z}_1}\quad r_2=-i\sqrt{\tilde{z}_1}\quad r_3=\sqrt{\tilde{z}_2}\quad r_4=-\sqrt{\tilde{z}_2} \tag{B8}$$

with which the solution is in the form

$$W(\xi)=C_1 e^{r_1\xi}+C_2 e^{r_2\xi}+C_3 e^{r_3\xi}+C_4 e^{r_4\xi} \tag{B9}$$

which can be transformed using Euler's identity to

$$W(\xi)=P_1\cos(\lambda_1\xi)+P_2\sin(\lambda_1\xi)+P_3\cosh(\lambda_2\xi)+P_4\sinh(\lambda_2\xi) \tag{B10}$$

with

$$\lambda_1=\sqrt{|\tilde{z}_1|}\quad and\quad \lambda_2=\sqrt{|\tilde{z}_2|}. \tag{B11}$$

Substituting this form of the solution into the boundary conditions, one obtains four equations, written in matrix form as

$$\boldsymbol{M}\cdot\boldsymbol{p}=\underline{0} \tag{B12}$$

with

$$\boldsymbol{p}^{\boldsymbol{T}}=\begin{bmatrix}\boldsymbol{P}_1 & \boldsymbol{P}_2 & \boldsymbol{P}_3 & \boldsymbol{P}_4\end{bmatrix} \tag{B13}$$

and

$$\boldsymbol{M}=\begin{bmatrix}
\eta_L & \lambda_1^3+(\nu+\eta_{LR})\lambda_1 & \eta_L & -\lambda_2^3+(\nu+\eta_{LR})\lambda_2\\
\lambda_1^2-\eta_{LR} & -\eta_R\lambda_1 & -\lambda_2^2-\eta_{LR} & -\eta_R\lambda_2\\
(\lambda_1^3+\nu\lambda_1)\sinh(\lambda_1)+\alpha\Omega^2\cosh(\lambda_1) & (\lambda_1^3+\nu\lambda_1)\cosh(\lambda_1)+\alpha\Omega^2\sinh(\lambda_1) & (\lambda_2^3-\nu\lambda_2)\sin(\lambda_2)+\alpha\Omega^2\cos(\lambda_2) & (-\lambda_2^3+\nu\lambda_2)\cos(\lambda_2)+\alpha\Omega^2 sin(\lambda_2)\\
\lambda_1^2\cosh(\lambda_1)-\beta\Omega^2\lambda_1\sinh(\lambda_1) & \lambda_1^2\sinh(\lambda_1)-\beta\Omega^2\lambda_1\cosh(\lambda_1) & -\lambda_2^2\cos(\lambda_2)+\beta\Omega^2\lambda_2\sin(\lambda_2) & -\lambda_2^2\sin(\lambda_2)-\beta\Omega^2\lambda_2\cos(\lambda_2)
\end{bmatrix} \tag{B14}$$

Looking for nontrivial solutions of this equation one obtains

$$det(M)=0 \tag{B15}$$

from which one can obtain the non-dimensional circular frequency Ω, and from that the natural frequency using

$$f_1=\frac{\omega}{2\pi}=\Omega c_0=\Omega\sqrt{\frac{m_T L_T^3}{EI_\eta}} \tag{B16}$$

The equation that has to be solved is transcendental and therefore solutions can only be obtained numerically.

Appendix C. – Tower idealisation

The towers of offshore wind turbines are tapered towers with diameters decreasing from the bottom to the top. Typically, the wall thickness of the tower also decreases with height. However, some small and medium sized turbines have constant wall thickness. The formulation presented in this paper replaces this tower shape with an equivalent constant diameter, constant wall thickness tower. The average tower diameter

$$D_T=\frac{D_b+D_t}{2} \tag{C1}$$

is used in combination with an equivalent tower wall thickness t_T. Note that if the average wall thickness is determined from a range

of wall thicknesses of the tower or from the mean of the top and bottom wall thicknesses, then the tower mass, as calculated from the idealised tower geometry,

$$m'_T = D_T \pi t_T \rho_T L_T \tag{C2}$$

may not be the same as the actual tower mass m_T. In the case that information about tower wall thickness is not available, the equivalent thickness can be chosen such that the actual tower mass is maintained, that is,

$$t_T = \frac{m_T}{L_T D_T \pi \rho_T} \tag{C3}$$

The non-dimensional stiffness parameters are normalised with the length L_T and the bending stiffness $E_T I_T$ of the tower. When calculating these non-dimensional stiffness parameters, the equivalent bending stiffness is calculated such that the deflection at the tower top due to a force acting perpendicular to the tower at the tower top is the same for the equivalent constant diameter tower as that of the tapered tower. The derivation is given here.

$$D_b = qD_t \tag{C4}$$

The diameter varies along the structure as

$$D(z) = \frac{D_t}{L_T}[L_T + (q-1)z] \tag{C5}$$

with $z=0$ at the top of the tower and positive downwards. The second moment of area is then given as

$$I_T(z) = \frac{1}{8}\pi D_T^3(z) t_T = \frac{1}{8}\pi \frac{D_t^3}{L_T^3} t_T [L_T + (q-1)z]^3 = I_t(1+az)^3 \tag{C6}$$

where

$$a = \frac{q-1}{L_T}. \tag{C7}$$

Moment curvature relation is written as

$$E_T I_T \frac{d^2 w}{dz^2} = Fz \tag{C8}$$

where F is the horizontal force at the hub. One can write

$$E_T I_t (1+az)^3 \frac{d^2 w}{dz^2} = Fz \tag{C9}$$

and from that w is obtained via integration

$$\frac{d^2 w}{dz^2} = \frac{Fz}{E_T I_t (1+az)^3} \tag{C10}$$

$$\frac{dw}{dz} = \frac{F}{E_T I_t a^2}\left[\frac{1}{2(1+az)^2} - \frac{1}{1+az}\right] + C_1 \tag{C11}$$

$$w = \frac{F}{E_T I_t a^2}\left[-\frac{1}{2a(1+az)^2} - \frac{\ln(1+az)}{a}\right] + C_1 z + C_2 \tag{C12}$$

The boundary conditions are used to calculate the constants.

$$z = L_T, \frac{dw}{dz} = 0 \quad C_1 = \frac{F}{E_T I_t a^2}\left[\frac{1}{1+aL_T} - \frac{1}{2(1+aL)^2}\right] \tag{C13}$$

$$z = L_T,\ w = 0$$

$$C_2 = \frac{F}{E_T I_t a^2}\left[\frac{\ln(1+aL_T)}{a} + \frac{1}{2a(1+aL_T)} - \frac{L_T}{1+aL_T} + \frac{L_T}{2(1+aL_T)^2}\right] \tag{C14}$$

The deflection at the end of the column is obtained by substituting $z=0$ into the equation of deflection

$$w_{free} = \frac{H}{E_T I_b a^2}\left[\frac{\ln(1+aL_T)}{a} + \frac{1}{2a(1+aL_T)} - \frac{L_T}{1+aL_T} + \frac{L_T}{2(1+aL_T)^2} - \frac{1}{2a}\right] \tag{C15}$$

$$w_{free} = \frac{FL^3}{E_T I_t}\left[\frac{q^2(2\ln q - 3) + 4q - 1}{2q^2(q-1)^3}\right] \tag{C16}$$

The stiffness is then given as

$$k = \frac{E_T I_b}{L_T^3}\left[\frac{2q^2(q-1)^3}{q^2(2\ln q - 3) + 4q - 1}\right] \tag{C17}$$

Verification: for a cantilever beam of constant diameter

$$\lim_{q\to 1}\left[\frac{2q^2(q-1)^3}{q^2(2\ln q - 3) + 4q - 1}\right] = 3 \tag{C18}$$

In the paper the following notification is used

$$E_T I_t = EI_t$$

Appendix D. – Guidance on the calculation of foundation stiffness

The stiffness of the foundation is used as input in the calculations shown in this paper. However, determining the stiffness is the most challenging task. In the absence of careful (very expensive) and detailed site measured data, existing formulations available in the literature may be used to estimate the stiffness of the foundation theoretically. For the sake of brevity only a brief summary of some common methods are presented here.

For static analysis, two methods are given in [42], one methodology based on a subgrade analysis approach partially based on Broms [16] and Broms [17] and another based on an elastic continuum approach. Results are provided for both cohesive and cohesionless soils, with simple analytical results available for slender (infinitely

Table D1
Approximation formulae based on soil conditions and pile slenderness.

	Slender pile	Rigid pile
Constant k_h [42]	$\begin{bmatrix} F \\ M \end{bmatrix} = \begin{bmatrix} \frac{k_h D_P}{\beta} & -\frac{k_h D_P}{2\beta^2} \\ -\frac{k_h D_P}{2\beta^2} & \frac{k_h D_P}{2\beta^3} \end{bmatrix} \begin{bmatrix} \rho \\ \theta \end{bmatrix}$	$\begin{bmatrix} F \\ M \end{bmatrix} = \begin{bmatrix} k_h D_P L & -\frac{k_h D_P L^2}{2} \\ -\frac{k_h D_P L^2}{2} & \frac{k_h D_P L^3}{3} \end{bmatrix} \begin{bmatrix} \rho \\ \theta \end{bmatrix}$
Linear k_h [42]	$\begin{bmatrix} F \\ M \end{bmatrix} = \begin{bmatrix} 1.077 \bullet n_h^{\frac{3}{5}} (E_P I_P)^{\frac{4}{5}} & -0.99 \bullet n_h^{\frac{2}{5}} (E_P I_P)^{\frac{3}{5}} \\ -0.99 \bullet n_h^{\frac{2}{5}} (E_P I_P)^{\frac{3}{5}} & 1.485 \bullet n_h^{\frac{1}{5}} (E_P I_P)^{\frac{4}{5}} \end{bmatrix} \begin{bmatrix} \rho \\ \theta \end{bmatrix}$	$\begin{bmatrix} F \\ M \end{bmatrix} = \begin{bmatrix} \frac{1}{2}L^2 n_h & -\frac{1}{3}L^3 n_h \\ -\frac{1}{3}L^3 n_h & \frac{1}{4}L^4 n_h \end{bmatrix} \begin{bmatrix} \rho \\ \theta \end{bmatrix}$
Bedrock – shear modulus G_S based [20,43]	$\begin{bmatrix} F \\ M \end{bmatrix} = \begin{bmatrix} 3.15 G^* D_P \left(\frac{E_P}{G^*}\right)^{\frac{1}{7}} & -0.53 G^* D_P^2 \left(\frac{E_P}{G^*}\right)^{\frac{3}{7}} \\ -0.53 G^* D_P^2 \left(\frac{E_P}{G^*}\right)^{\frac{3}{7}} & 0.25 G^* D_P^3 \left(\frac{E_P}{G^*}\right)^{\frac{5}{7}} \end{bmatrix} \begin{bmatrix} \rho \\ \theta \end{bmatrix}$	$\begin{bmatrix} F \\ M \end{bmatrix} = \begin{bmatrix} \frac{3.15 G^* D_P^{\frac{2}{7}} L^{\frac{1}{7}}}{1-0.28\left(\frac{2L}{D_P}\right)^{\frac{1}{4}}} & -\frac{2 G^* D_P^{\frac{7}{8}} L^{\frac{9}{8}}}{1-0.28\left(\frac{2L}{D_P}\right)^{\frac{1}{4}}} \\ -\frac{2 G^* D_P^{\frac{7}{8}} L^{\frac{9}{8}}}{1-0.28\left(\frac{2L}{D_P}\right)^{\frac{1}{4}}} & \frac{4 G^* D_P^{\frac{4}{7}} L^{\frac{5}{7}}}{1-0.28\left(\frac{2L}{D_P}\right)^{\frac{1}{4}}} \end{bmatrix} \begin{bmatrix} \rho \\ \theta \end{bmatrix}$

long) and rigid (infinitely stiff) piles. Another static stiffness approach is recommended in Eurocode 8 Part 5 [26] based on Gazetas [27], developed for seismic analysis of slender piles.

Dynamic analysis using a subgrade reaction approach of a beam on an elastic foundation was developed in terms of p-y curves [37,39,41,44,5], which is the currently accepted design procedure suggested by e.g. the DNV code for offshore wind turbines [25]. This methodology is based on Winkler's approach [53] and utilises non-linear springs to model the elastic foundation. Analytical solutions for dynamic analysis have been published by e.g. Nogami and Novak [38,40]. Green's function based models have also been developed for dynamic stiffness of piles, e.g. [29,31]. Recent work regarding dynamic stiffness and damping of monopiles of offshore wind turbines include Shadlou and Bhattacharya [45], Zania [56] and Damgaard et al. [23]. For seismic analysis, a three-step solution was suggested by Kausel et al. [30], including simplified approximate expressions that make the method more attractive than finite element analysis. Finite element based methods for analysis of piles were developed by e.g. Blaney et al. [15].

In this appendix, however, the simple formulae in [42,43,20] are used. These formulations neglect the frequency dependence of foundation stiffness, which can be justified for dynamic loading of offshore wind turbines because the frequencies of excitation are so low. For seismic analysis, however, this frequency dependence should be taken into account. These approximations provide quick and easy solutions for foundation stiffness, achieving sufficiently accurate results for the natural frequency as shown in the paper.

The two main parameters to decide the calculation methodology for foundation stiffness are:

(1) Soil condition and ground profile at the site and
(2) Pile slenderness/rigidity.

The ground type/ soil determines the main soil parameter for estimating soil stiffness, while determining whether the pile can be considered slender or rigid. This allows for simplification of the foundation stiffness estimation and for the use of closed form solutions instead of graphs or numerical methods.

Ground profile and soil conditions at the site

There are three main categories to consider from the point of view of the current analysis.

(1) Cohesive soils: the horizontal modulus of subgrade reaction k_h is considered constant with depth below the mudline. This is typically used for over-consolidated clayey soils which is often encountered in offshore conditions, see Bhattacharya et al., [14]) for typical North Sea soils. For normally consolidated cohesive soils, the subgrade reaction increases linearly with depth.
(2) Cohesionless soils: the horizontal modulus of subgrade reaction k_h is assumed to increase with the square root of the depth below the mudline. This can be typically used for loose to medium dense sand and gravels.
(3) Bedrock: The foundation stiffness is determined by the shear modulus of the soil. This is typically used for weathered bedrock and very dense sand.
(4) Complex layered soils: For real sites the soil is obviously not always as simple as the above categories and different layers are often observed. One of the above categories may be chosen for such complex sites, bearing in mind that from the point of view of pile head deflection/rotation and pile stiffness the upper layers of the soil are of higher importance, and the upper layers should be weighted accordingly. The soil types at the sites of all the wind turbines considered in this paper are listed in Table 1 in Section 1. Alternatively, the stiffness can be more accurately obtained from p-y curves.

The constant horizontal modulus of subgrade reaction k_h for cohesive soils can be determined using the expression of Vesic [52], using the parameters from Tables 6 and 7:

$$k_h = \frac{0.65}{D_P}\sqrt[12]{\frac{E_S D_P^4}{E_P I_P}}\left(\frac{E_S}{1-\nu_S^2}\right) \tag{D1}$$

where I_P is the second moment of area of the pile cross section E_S is the elastic modulus of the soil, and ν_S is the soil's Poisson's ratio. Broms [17] provides another expression for clays based on the secant Young's modulus E_{50}

$$k_h = \frac{1.67E_{50}}{D_P} \tag{D2}$$

which can be used in combination with the formula of Skempton [47] or the more conservative formula of Davisson [24] as quoted in [42], in terms of the undrained shear strength c_u

$$\text{Skempton}: E_{50} = (50-200)\cdot c_u \text{ and } k_h = (80-320)\cdot\frac{c_u}{D_P}$$
$$\text{Davisson}: k_h = 67\cdot\frac{c_u}{D_P} \tag{D3}$$

The linearly varying modulus of subgrade reaction of cohesionless soils can be written following [42] as:

$$k_h = n_h\cdot\frac{z}{D_P} \tag{D4}$$

where n_h is the coefficient of subgrade reaction, calculated for sand after [49] as

$$n_h = \frac{A\cdot\gamma_{\text{sand}}}{1.35} \tag{D5}$$

where γ_{sand} is the specific weight of sand and $A = 100-300$ for loose sand, $A = 300-1000$ for medium sand, and $A = 1000-2000$ for dense sand. The modulus of subgrade reaction k_h for cohesive soils and the coefficient of subgrade reaction n_h for cohesionless soils are used to calculate the foundation stiffness, as given in Table D1. In Table D1 ρ and θ are mudline pile head deflection and rotation, respectively, F and M are horizontal force and overturning moment at the mudline.

Slenderness/rigidity of the pile

Simple closed form solutions are readily available for the simplified cases obtained by assuming either a slender pile or a rigid pile.

(1) Slender pile: The monopile is idealised as 'slender' or 'infinitely long' assuming that the pile flexibly deflects and that the pile fails first by yielding through a plastic hinge (as opposed to failure of the soil).
(2) Rigid pile: The monopile is idealised as 'rigid' or 'infinitely stiff' assuming that the pile undergoes rigid body rotation (the soil fails first). However significant bending moment may be generated in the pile

Two main methods are presented here to determine whether a pile can be slender or rigid. The first one is given in [42] and is based on the modulus of subgrade reaction k_h and the bending stiffness of the pile $E_P I_P$. The slenderness parameter is calculated as

$$\beta = \sqrt[4]{\frac{k_h D_P}{4E_P I_P}} \tag{D6}$$

The pile is considered slender or infinitely long if $\beta L_P > 2.5$, and considered rigid if $\beta L_P < 1.5$.

The second method is that of Randolph [43] and Carter and Kulhawy [20], which is based on the equivalent Young's modulus

E_e of the pile, and the effective shear strength of the soil G^*.

$$E_e = \frac{E_P I_P}{D_P^4 \pi/64}; \qquad G^* = G_S\left(1+\frac{3}{4}\nu_S\right) \tag{D7}$$

where G_S is the shear modulus of the soil. The pile is considered

$$\text{slender, if} \quad \frac{L_P}{D_P} \geq \left(\frac{E_e}{G^*}\right)^{\frac{2}{7}} \tag{D8}$$

$$\text{rigid, if} \quad \frac{L_P}{D_P} \leq 0.05\left(\frac{E_e}{G^*}\right)^{\frac{1}{2}}. \tag{D9}$$

This methodology is used for rocks by Carter and Kulhawy [20]. The formulae summarised in Table D1 were used to approximate the foundation stiffness in the present study and were found to provide good approximations in terms of natural frequency. The difference between the rigid and slender pile approximations is typically 1–6%.

References

[1] 4C Offshore Limited. Global offshore wind farms database. In: 4COffshore.com web page. ⟨http://www.4coffshore.com/windfarms/⟩; 2015 [accessed 19.03.15].
[2] 4C Offshore Limited. Offshore wind turbine database. In: 4COffshore.com web page. ⟨http://www.4coffshore.com/windfarms/turbines.aspx⟩; 2015 [accessed 19.03.15].
[3] Adhikari S, Bhattacharya S. Dynamic analysis of wind turbine towers on flexible foundations. Shock Vib 2012;19:37–56.
[4] Adhikari S, Bhattacharya S. Vibrations of wind-turbines considering soil–structure interaction. Wind Struct 2011;14:85–112.
[5] API. Recommended practice for planning, designing and constructing fixed offshore platforms—working stress design; 2005.
[6] Arany L, Bhattacharya S, Adhikari S, Macdonald John HG, Hogan S John. An analytical model to predict the natural frequency of offshore wind turbines on three-spring flexible foundations using two different beam models. Soil Dyn Earthq Eng 2015;74:40–5. http://dx.doi.org/10.1016/j.soildyn.2015.03.007.
[7] Arany L, Bhattacharya S, Hogan SJ, Macdonald J. Dynamic soil–structure interaction issues of offshore wind turbines. In: Proceedings of the 9th international conference on structural dynamics EURODYN; 2014. p. 3611–8.
[8] Arany L, Bhattacharya S, Macdonald J, Hogan SJ. Simplified critical mudline bending moment spectra of offshore wind turbine support structures. Wind Energy 2015;18(12):2171–97. http://dx.doi.org/10.1002/we.1812.
[9] Bhattacharya S. SDOWT: user manual (simplified dynamics of wind turbines); 2011. 1–51.
[10] Bhattacharya S, Adhikari S. Experimental validation of soil–structure interaction of offshore wind turbines. Soil Dyn Earthq Eng 2011;31:805–16. http://dx.doi.org/10.1016/j.soildyn.2011.01.004.
[11] Bhattacharya S, Cox JA, Lombardi D, Wood DM. Dynamics of offshore wind turbines supported on two foundations. Proc ICE – Geotech Eng 2013;166:159–69. http://dx.doi.org/10.1680/geng.11.00015.
[12] Bhattacharya S, Nikitas N, Garnsey J, Alexander N, Cox J, Lombardi D, Wood DM, Nash David FT. Observed dynamic soil–structure interaction in scale testing of offshore wind turbine foundations. Soil Dyn Earthq Eng 2013;54:47–60.
[13] S. Bhattacharya, Challenges in design of foundation for offshore wind turbines, Engineering & Technology Reference, 01 January 2012, 9 pp. http://dx.doi.org/10.1049/etr.2014.0041, Online ISSN 2056-4007.
[14] Bhattacharya S, Carrington T, Aldridge T. Observed increases in offshore pile driving resistance. Proceedings of the Institution of Civil Engineers - Geotechnical Engineering 2009;162(1):71–80. http://dx.doi.org/10.1680/geng.2009.162.1.71.
[15] Blaney GW, Kausel E, Roesset JM. Dynamic stiffness of piles. In: Proceedings of the 2nd international conference on numerical methods in geomechanics. Blacksburg, Virginia; 1976. p. 1001–12.
[16] Broms BB. Lateral resistance of pile in cohesionless soils. J Soil Mech Found Div ASCE 1964;90:123–56.
[17] Broms BB. Lateral resistance of pile in cohesive soils. J Soil Mech Found Div ASCE 1964;90:27–64.
[18] Burton T, Sharpe D, Jenkins N, Bossanyi E. Wind energy handbook, 2nd edition; 2011. http://dx.doi.org/10.1002/0470846062.
[19] Camp TR, Morris MJ, van Rooij R, van der Tempel J, Zaaijer M, Henderson A, Argyriadis M, Swartz S, Just H, Grainger W, Pearce D. Design methods for offshore wind turbines at exposed sites (final report of the OWTES project EU Joule III project JOR3-CT98-0284). Bristol; 2004.
[20] Carter J, Kulhawy F. Analysis of laterally loaded shafts in rock. J Geotech Eng 1992;118:839–55.
[21] Damgaard M, Andersen J. Natural frequency and damping estimation of an offshore wind turbine structure. In: Proceedings of the 22nd international offshore and polar engineering conference. Rhodes, Greece; 2012. p. 300–7.
[22] Damgaard M, Ibsen LB, Andersen LV, Andersen JKF. Cross-wind modal properties of offshore wind turbines identified by full scale testing. J Wind Eng Ind Aerodyn 2013;116:94–108. http://dx.doi.org/10.1016/j.jweia.2013.03.003.
[23] Damgaard M, Zania V, Andersen L, Ibsen LB. Effects of soil–structure interaction on real time dynamic response of offshore wind turbines on monopiles. Eng Struct 2014;75:388–401. http://dx.doi.org/10.1016/j.engstruct.2014.06.006.
[24] Davisson MT. Lateral load capacity of piles. Highw Res Rec 333, 1970:104–12.
[25] DNV. Offshore standard DNV-OS-J101 design of offshore wind turbine structures. Høvik, Norway; 2014.
[26] European Committee for Standardization. Eurocode 8: design of Structures for earthquake resistance—part 5: foundations, retaining structures and geotechnical aspects; 2003.
[27] Gazetas G. Seismic response of end-bearing single piles. Int J Soil Dyn Earthq Eng 1984;3:82–93. http://dx.doi.org/10.1016/0261-7277(84)90003-2.
[28] Kallehave D, Thilsted CL. Modification of the API p-y formulation of initial stiffness of sand. Offshore site investigation and geotechnics: integrated geotechnologies – present and future; 2012.
[29] Kausel E. An explicit solution for the Green functions for dynamic loads in layered media. Cambridge, MA 02139; 1981.
[30] Kausel E, Whitman RV, Morray JP, Elsabee F. The spring method for embedded foundations. Nucl Eng Des 1978;48:377–92. http://dx.doi.org/10.1016/0029-5493(78)90085-7.
[31] Kaynia AM. Dynamic stiffness and seismic response of pile groups. Cambridge, Massachusetts: Massachusetts Institute of Technology; 1982.
[32] Kühn M. Soft or stiff: a fundamental question for designers of offshore wind energy converters. In: Proceedings of the European wind energy conference EWEC'97; 1997.
[33] Leblanc Thilsted C, Tarp-Johansen NJ. Monopiles in sand—stiffness and damping. In: Proceedings of the European wind energy conference; 2011.
[34] Lindoe Offshore Renewables Center. Offshore wind farm knowledge base. In: lorc.dk web page. ⟨⟨http://www.lorc.dk/knowledge⟩⟩; 2011 [accessed 19.03.15].
[35] Lombardi D, Bhattacharya S, Wood D Muir. Dynamic soil–structure interaction of monopile supported wind turbines in cohesive soil. Soil Dyn Earthq Eng 2013;49:165–80. http://dx.doi.org/10.1016/j.soildyn.2013.01.015.
[36] Lowe J. Hornsea met mast—a demonstration of the "twisted jacket" design. In: Proceedings of the global offshore wind conference; 2012.
[37] Matlock H. Correlations for design of laterally loaded piles in soft clay. In: Proceedings of the second annual offshore technology conference; 1970.
[38] Nogami T, Novak M. Resistance of soil to a horizontally vibrating pile. Earthq Eng Struct 1977;5:249–61.
[39] Novak M. Dynamic stiffness and damping of piles. Can Geotech J 1974;11:574–98.
[40] Novak M, Nogami T. Soil–pile interaction in horizontal vibration. Earthq Eng Struct Dyn 1977;5:263–81. http://dx.doi.org/10.1002/eqe.4290050305.
[41] O'Neill MW, Murchinson JM. An evaluation of p-y relationships in sands; 1983.
[42] Poulos H, Davis E. Pile foundation analysis and design. New York: Rainbow-Bridge Book Co., Wiley; 1980.
[43] Randolph MF. The response of flexible piles to lateral loading. Géotechnique 1981;31:247–59.
[44] Reese LC, Cox WR, Koop FD. Field testing and analysis of laterally loaded piles in stiff clay. In: Proceedings of the seventh annual offshore technology conference; 1975.
[45] Shadlou M, Bhattacharya S. Dynamic stiffness of pile in a layered elastic continuum. Géotechnique 2014;64:303–19.
[46] Shirzadeh R, Devriendt C, Bidakhvidi MA, Guillaume P. Experimental and computational damping estimation of an offshore wind turbine on a monopile foundation. J Wind Eng Ind Aerodyn 2013;120:96–106. http://dx.doi.org/10.1016/j.jweia.2013.07.004.
[47] Skempton AW. The bearing capacity of clays; 1951.
[48] Tarp-johansen NJ, Andersen L, Christensen ED, Mørch C, Kallesøe B, Frandsen S. Comparing sources of damping of cross-wind motion. In: Proceedings of the European wind energy conference; 2009.
[49] Terzaghi K. Evaluation of coefficient of subgrade reaction. Geotechnique 1955;5:41–50.
[50] van der Tempel J, Molenaar DP. Wind turbine structural dynamics—a review of the principles for modern power generation, onshore and offshore. Wind Eng 2002;26:211–20.
[51] Versteijlen WG, Metrikine AV, Hoving JS, de Vries WE. Estimation of the vibration decrement of an offshore wind turbine support structure caused by its interaction with soil. In: Proceedings of the EWEA offshore conference; 2011.
[52] Vesic AB. Bending of beams resting on isotropic elastic solid. J Eng Mech Div 1961;87:35–54.
[53] Winkler E. Die Lehre Von der Elasticitaet und Festigkeit. H. Dominicus, Prag; 1867.
[54] Zaaijer M. Design methods for offshore wind turbines at exposed sites (OWTES)—sensitivity analysis for foundations of offshore wind turbines. Delft, The Netherlands; 2002.
[55] Zaaijer MB. Foundation models for the dynamic response of offshore wind turbines; 2002.
[56] Zania V. Natural vibration frequency and damping of slender structures founded on monopiles. Soil Dyn Earthq Eng 2014;59:8–20. http://dx.doi.org/10.1016/j.soildyn.2014.01.007.